

## Supporting Information

### Nanopump for Low-temperature and Efficient Solar Water Evaporation

Yujie Zhao<sup>a</sup>, Kaiqi Zhao<sup>b</sup>, Junwen Yin<sup>c</sup>, Jieying Yang<sup>a</sup>, Jie Xu<sup>d</sup>, Yizhuo Gu<sup>a</sup>, Limin Liu<sup>e</sup>, Jun Luo<sup>d</sup>,

Yan Li<sup>a\*</sup> Lidong Sun<sup>b\*</sup>

<sup>a</sup> School of Materials Science and Engineering, Beihang University, Beijing 100010, China

E-mails: [liyan@buaa.edu.cn](mailto:liyan@buaa.edu.cn)

<sup>b</sup> School of Materials Science and Engineering, Chongqing University, Chongqing 400044, China

E-mails: [lidong.sun@cqu.edu.cn](mailto:lidong.sun@cqu.edu.cn)

<sup>c</sup> Beijing Computational Science Research Center, Beijing 100084, China

<sup>d</sup> Center for Electron Microscopy and Tianjin Key Lab of Advanced Functional Porous Materials, Institute for New Energy Materials & Low-Carbon Technologies, School of Materials Science and Engineering, Tianjin University of Technology, Tianjin 300384, China

<sup>e</sup> School of Physics, Beihang University, Beijing 100191, China

---

\* Corresponding authors,

E-mail addresses: [liyan@buaa.edu.cn](mailto:liyan@buaa.edu.cn) (Y. Li), [lidong.sun@cqu.edu.cn](mailto:lidong.sun@cqu.edu.cn) (L. Sun)

# **S1. Experimental Section**

## **S1.1 Sample preparation**

The Zr-30Ti alloy ingots were prepared by a non-consumable arc-melting method under Ar atmosphere protection, using high purity titanium (99.9 wt%) and zirconium (99.9 wt%). The obtained alloys were sealed in a glass tube with Ar, and then annealed with furnace cooling to reduce composition segregation and ensure compositional homogeneity. Specimens for electrochemical anodization were cut into slices of  $10 \times 15 \times 0.7 \text{ mm}^3$  and polished with silicon carbide abrasive paper up to #3000. The polished samples were rinsed in acetone and ethanol sequentially, followed by washing with deionized water and drying in oven at  $50 \text{ }^\circ\text{C}$  for 30 min.

## **S1.2 Electrochemical anodization**

Electrochemical anodization was carried out in a two-electrode configuration with the Zr-30Ti alloy as the working electrode and the platinum as the counter electrode. A programmable DC power supply (Keithley 2200-72-1) was used to provide anodization voltage of 30 V. The electrolyte solution was ethylene glycol containing 0.5 wt%  $\text{NH}_4\text{F}$  and 5 vol% deionized water. After anodization, the samples were rinsed with deionized water and dried in air. The as-prepared samples were annealed in a tube furnace at  $450 \text{ }^\circ\text{C}$  for 1 h in air. The nanotube membranes were thus obtained, which were peeled off naturally from the alloy substrate after annealing, as shown in Figure S1. This is due to the difference in coefficient of thermal expansion between metal substrate and oxide coating. The membranes of  $\text{Zr}(\text{Ti})\text{O}_2$  nanoparticles were prepared by annealing at  $1000 \text{ }^\circ\text{C}$  for 6 h.

## **S1.3 Characterization**

The morphology of the membranes was observed by scanning electron microscopy (SEM, Zeiss-Supra55) and transmission electron microscopy (TEM, Tecnai F20). The microstructure was characterized by scanning transmission electron microscopy (STEM, Titan Cubed Themis G2 300). The atomic composition was investigated using scanning electron microscopy and transmission electron microscopy with energy dispersive X-ray spectroscopy (EDX). The X-ray diffraction (XRD) patterns were recorded on D/Max 2500 PC X-ray spectrometer with  $\text{Cu K}\alpha$  radiation ( $\lambda=1.5406 \text{ \AA}$ )

at a scanning speed of  $6^\circ \text{ min}^{-1}$ . The elemental composition was analyzed by X-ray photoelectron spectroscopy (XPS, AEM PHI5300, Japan). The contact angles of nanotubes were recorded with a standard contact-angle analyzer (Dataphysics OCA 15EC). The spectra measurements from 220-2500 nm were performed to assess the absorption capability of nanotubes using UV-vis spectrophotometry (UV-3600, Japan).

The electron spin resonance (ESR) measurement was performed at  $198^\circ \text{C}$  using an ESR spectrometer (Bruker A300, Germany). The ESR spectra were recorded using 18.92 mW microwave power and 9.86 GHz microwave frequency. The g factor is calculated using the following equation:<sup>1</sup>

$$g = \frac{h\nu}{\beta B} \quad \text{Equation S1}$$

Where  $\beta$  is the constant (Bohr magneton),  $h$  is the Planck constant,  $\nu$  is the microwave frequency, and  $B$  is the magnetic field.

#### **S1.4 Density functional theory (DFT) calculations**

Spin-polarized periodic calculations implemented in the CP2K/Quickstep package were performed to investigate the atomic and electronic structure of  $\text{ZrO}_2$  and  $\text{Zr}(\text{Ti})\text{O}_2$ .<sup>2</sup> The norm-conserving Goedecker, Teter, and Hutter (GTH) pseudopotentials were used to describe core electrons.<sup>3</sup> Gaussian function with molecularly optimized triple-zeta polarized basis sets (m-TZVP) were adopted for expanding the wave function of Zr  $4s^2 4p^6 4d^2 5s^2$ , O  $2p^2 2p^4$ , Ti  $3s^2 3p^6 3d^2 4s^2$ .<sup>4</sup> We applied a 3.5 eV Hubbard U correction and a 2.9 eV Hubbard U correction to Ti 3d and Zr 4d orbitals, respectively, to evaluate the on-site Coulomb interactions in localized orbitals and exchange interactions. For the auxiliary basis set of plane waves, a 280 Ry cut-off was used, and all the atomic positions were fully relaxed until the force was smaller than  $0.02 \text{ eV}/\text{\AA}$ . The whole calculation was based on a 96-atom supercell of monoclinic  $\text{ZrO}_2$ . The optimized lattice parameters of monoclinic  $\text{ZrO}_2$  are  $a = 5.19 \text{ \AA}$ ,  $b = 5.24 \text{ \AA}$ ,  $c = 5.38 \text{ \AA}$ ,  $\beta = 99.69^\circ$ .

#### **S1.5 Solar water evaporation**

All of the solar water evaporation experiments were conducted using the same solar simulator (Perfectlight, CHF-XM500) accompanied by adjustable optical components. The solar illumination was monitored using the radiative meter (FZ-A) and controlled at  $1 \text{ kW m}^{-2}$ . A piece of  $\text{Zr(Ti)O}_2$  membrane was placed on top of a polyethylene foam column (height: 2 cm, diameter: 1.5 cm) wrapped by filter paper, which was floated on water in a 10 mL beaker. The beaker was wrapped by a polyethylene foam to reduce heat loss. The  $\text{Zr(Ti)O}_2$  membrane within a beaker was placed on an electronic calibrated balance (Aohaosi, ZH220H, accuracy: 0.1 mg) to record the real-time weight loss of water, which was used for measuring the evaporation rate. The exposed area under irradiation was about  $1 \text{ cm}^2$ . Meanwhile, the irradiated surface temperature of bare water,  $\text{ZrO}_2$  nanotubes,  $\text{Zr(Ti)O}_2$  nanotubes and  $\text{Zr(Ti)O}_2$  nanoparticles were measured using an infrared thermal imager (Fotric 226-3). For reliability test, the temperature was changed between  $8 \text{ }^\circ\text{C}$  and  $22 \text{ }^\circ\text{C}$  while the relative humidity was ranged from 20% to 60%.

For solar desalination, the water purity was measured using a multimeter with a constant distance between electrodes. The concentration of  $\text{Na}^+$  ions in purified water was measured by inductively coupled plasma mass spectrometry (PerkinElmer NexION 300D).

## S2. Equivalent Evaporation Enthalpy

It is reported that the vaporization enthalpy of water in porous structure is lower than that of bulk water ( $\sim 2256 \text{ J g}^{-1}$ ).<sup>5-7</sup> Accordingly, control experiments were carried out to estimate the vaporization enthalpy of water in  $\text{Zr(Ti)O}_2$  membranes. Two same beakers of 10 mL were employed as the containers, which were filled with the same amount of water. One beaker was equipped with the solar evaporation device using  $\text{Zr(Ti)O}_2$  membranes. Both beakers were covered with aluminum foils and wrapped up with polyethylene foams. The two devices were simultaneously placed in an electronic balance at room temperature ( $18\text{--}22^\circ \text{C}$ ) and ambient pressure. The electronic balance was surrounded with windshield to avoid the effect of air convection on the evaporation rate. The experiments were conducted in dark for more than 6 h, and the mass change of each beaker was recorded to calculate the solar evaporation under dark condition. The above experiments were repeated for 8 times and the evaporation rates were calculated and presented in **Table S1**.

**Table S1.** The evaporation rate of bare water and that with  $\text{Zr(Ti)O}_2$  membranes under dark condition.

Test	Evaporation rate of bare water ( $\text{kg m}^{-2} \text{ h}^{-1}$ )	Evaporation rate with $\text{Zr(Ti)O}_2$ membranes ( $\text{kg m}^{-2} \text{ h}^{-1}$ )	Evaporation rate ratio (bare water/ $\text{Zr(Ti)O}_2$ )
1	0.1610	0.2383	0.6756
2	0.1747	0.2440	0.7159
3	0.1764	0.2540	0.6933
4	0.1779	0.2579	0.6894
5	0.1820	0.2699	0.6743
6	0.2070	0.2990	0.6923
7	0.2110	0.3020	0.6986
8	0.2120	0.3142	0.6747

The equivalent evaporation enthalpy ( $E_{\text{equ}}$ ) of water in  $\text{Zr(Ti)O}_2$  membranes was estimated by vaporizing the water with identical power input ( $U_{\text{in}}$ ),<sup>6</sup>

$$U_{\text{in}} = E_{\text{water}} m_{\text{water}} = E_{\text{equ}} m_{\text{Zr(Ti)O}_2} \quad \text{Equation S2}$$

where  $E_{\text{water}}$  and  $m_{\text{water}}$  are the vaporization enthalpy and mass change of bare water, respectively;  $m_{\text{Zr(Ti)O}_2}$  is the mass change of Zr(Ti)O<sub>2</sub> membranes. Thus, the equivalent vaporization enthalpy of water in Zr(Ti)O<sub>2</sub> can be estimated as

$$E_{\text{equ}} = \frac{E_{\text{water}} m_{\text{water}}}{m_{\text{Zr(Ti)O}_2}} \quad \text{Equation S3}$$

Using the reported vaporization enthalpy of pure water (~2256 J g<sup>-1</sup>), the equivalent vaporization enthalpy of water in Zr(Ti)O<sub>2</sub> can be determined to be 1555 J g<sup>-1</sup> based on the data in Table S1. The reduced vaporization enthalpy of water in Zr(Ti)O<sub>2</sub> may be ascribed to the three-dimensional structure of the nanotube arrays and the high surface area produced. Because of the Zr(Ti)O<sub>2</sub> nanotubes, the heat transfer and mass transport processes are enhanced as compared to the bare water.

### S3. Estimation of Heat Loss

Under steady-state condition, the heat loss consists of conduction, radiation and convection.<sup>8-10</sup> The surface area of the Zr(Ti)O<sub>2</sub> membranes was about 1 cm<sup>2</sup> and the irradiation power input was kept constant. The weight of water was about 5 g. The temperature of the water before and after solar evaporation was 23.2 ° C and 27.0 ° C, respectively. The surface temperature of Zr(Ti)O<sub>2</sub> membrane was about 40.0 ° C. The temperature of vapor and the surrounding environment were about 35.8 ° C and 33.3 ° C, respectively. Calculations for the three components are as follows:

#### (1) Conduction Heat

The conduction heat can be calculated as follows<sup>8</sup>

$$Q_{\text{cond}} = Cm\Delta T \quad \text{Equation S4}$$

where  $C$  is the specific heat capacity of pure water,  $m$  stands for the weight of water and  $\Delta T$  is the elevated water temperature within 3600 s.

#### (2) Radiation Heat

It is calculated by the Stefan-Boltzmann equation.<sup>11</sup>

$$Q_{\text{radd}} = \varepsilon A\sigma(T_{\text{film}}^4 - T_{\text{vapor}}^4) \quad \text{Equation S5}$$

where  $\varepsilon$  is the emissivity,  $A$  denotes the surface area, and  $\sigma$  is the Stefan-Boltzmann constant ( $5.67 \times 10^{-8} \text{ W m}^{-2} \text{ K}^{-4}$ ),  $T_{\text{film}}$  is the temperature of absorber surface,  $T_{\text{vapor}}$  is the temperature of evaporated vapor.

#### (3) Convection Heat

It is defined by Newton' law of cooling.<sup>9</sup>

$$Q_{\text{conv}} = hA(T_{\text{film}} - T_{\text{envi}}) \quad \text{Equation S6}$$

where  $h$  is the convection heat transfer coefficient,  $A$  is the film area,  $T_{\text{envi}}$  is the temperature of surrounded environment.

Therefore, the heat loss can be calculated and the results are shown in **Table S2**.

**Table S2.** The calculated heat loss of Zr(Ti)O<sub>2</sub> membranes under 1 sun irradiation.

	Conduction heat loss	Radiation heat loss	Convection heat loss
Calculation value (%)	22.17	2.86	3.35

Accordingly, the total heat loss is calculated to be about 28.38%. The experimental total heat loss is about 29.16%. This indicates the reliability of our experiments.

For our nanotube membranes, with the measured wall temperature at the nanotubes, the mean temperature of water at inlet, local heat transfer coefficient of nanofluids and flow rate, the heat quantity is calculated by Newton's law of cooling as<sup>12</sup>

$$Q = A \times t \times h(x) \times \{T_s(x) - T_m(x)\} \quad \text{Equation S7}$$

where  $A$ ,  $t$ ,  $h(x)$ ,  $T_s(x)$ , and  $T_m(x)$  are the heat surface area, time, local heat transfer coefficient, the mean temperature of fluid and tube wall temperature.<sup>13-15</sup> In this work, we presume  $h(x)$  to be known, the heat quantity is proportional to the surface area. The high surface area of nanotubes can ensure sufficient contacts between solid and liquid at the interface, thus enhancing the heat transfer between tube walls and water molecules.

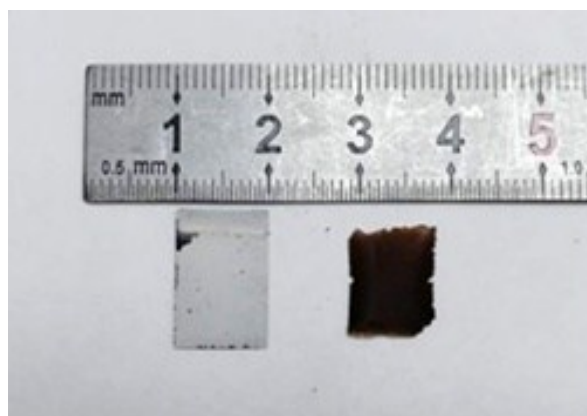


**Figure S1.** The optical photograph of free-standing  $\text{Zr}(\text{Ti})\text{O}_2$  nanotube membrane (the black one on the right) obtained by anodization and subsequently detached from the Zr-30Ti alloy substrate (the white one on the left).

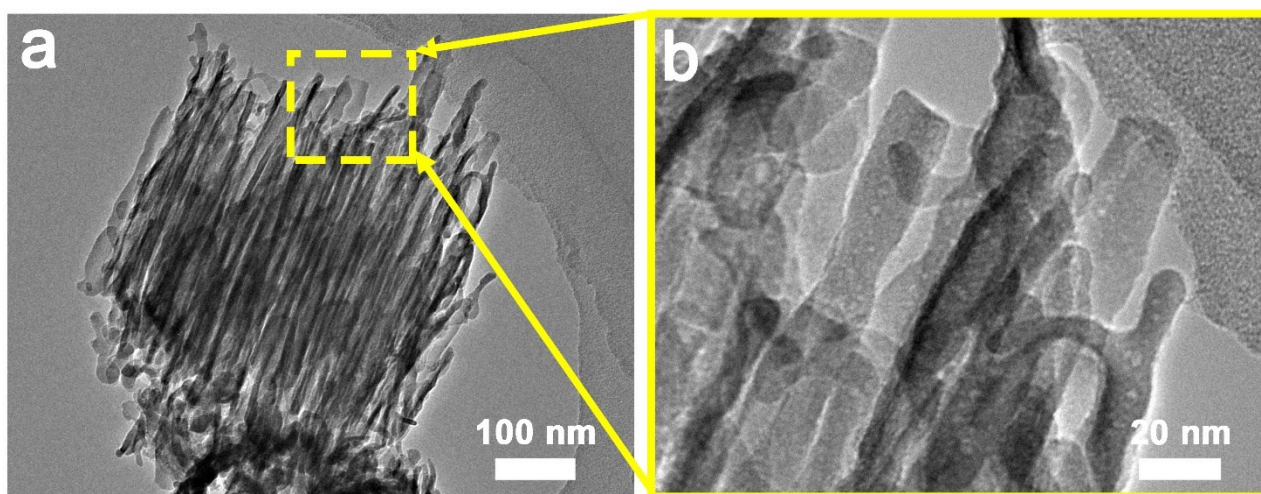


**Figure S2.** The TEM (a) and HRTEM (b) images of  $\text{Zr}(\text{Ti})\text{O}_2$  nanotubes showing the pinholes at tube walls.

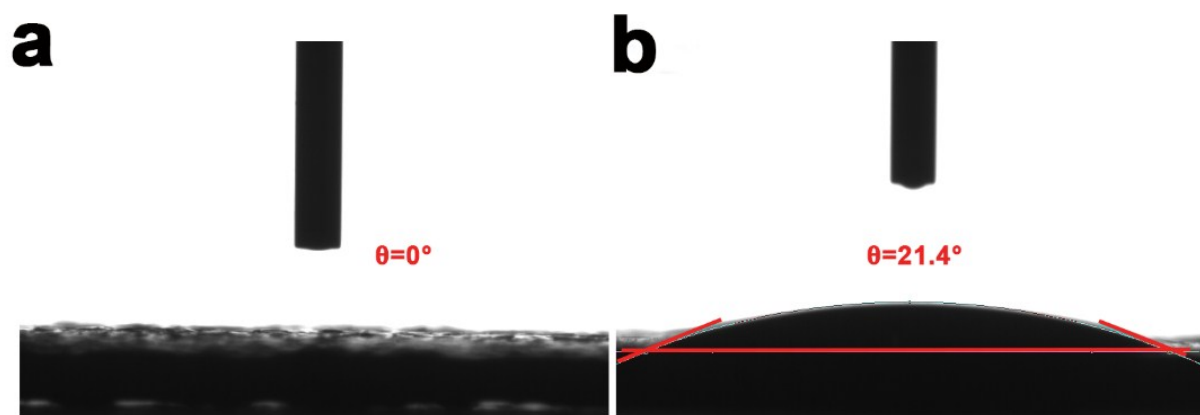


**Figure S3.** Water contact angle of  $\text{Zr(Ti)O}_2$  (a) and  $\text{ZrO}_2$  (b) membranes. The small contact angle in (a) is due to the rapid infiltration of the water droplet on the  $\text{Zr(Ti)O}_2$  membranes.

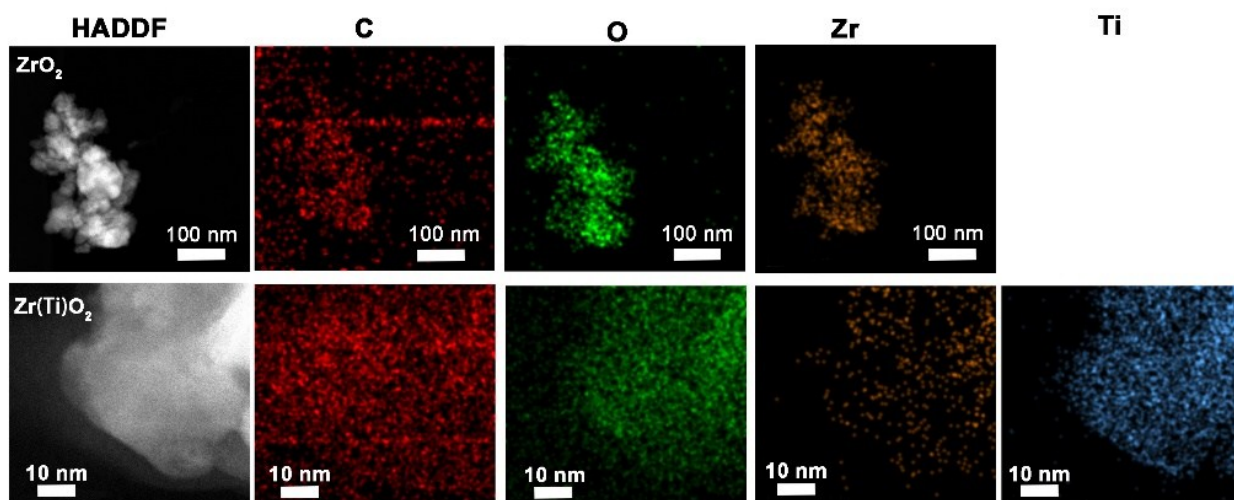


**Figure S4.** The HADDF STEM images and EDX mapping of  $\text{ZrO}_2$  (top row) and  $\text{Zr(Ti)O}_2$  (bottom row) after annealing at 700 °C.

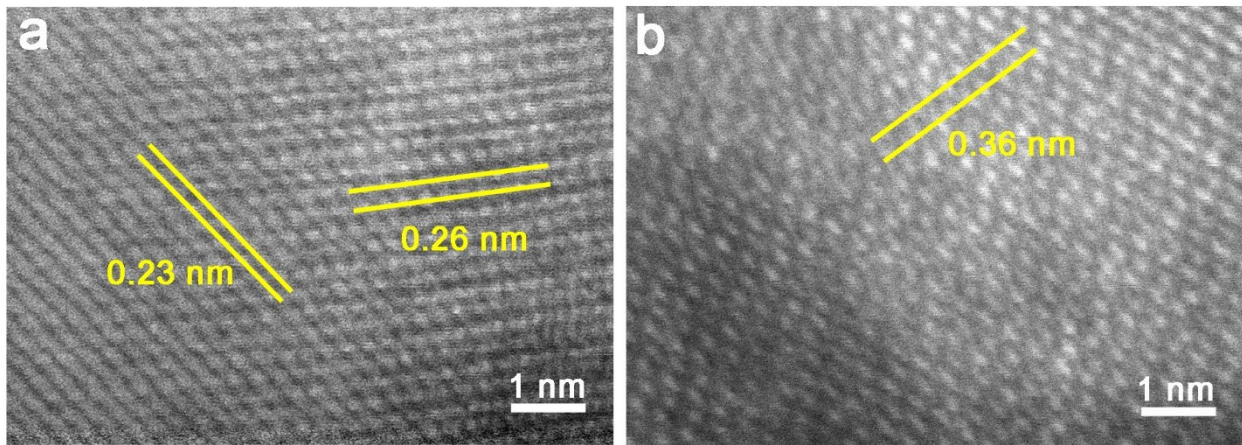


**Figure S5.** The STEM images of  $\text{Zr(Ti)O}_2$  after annealing at 700 °C for different positions.

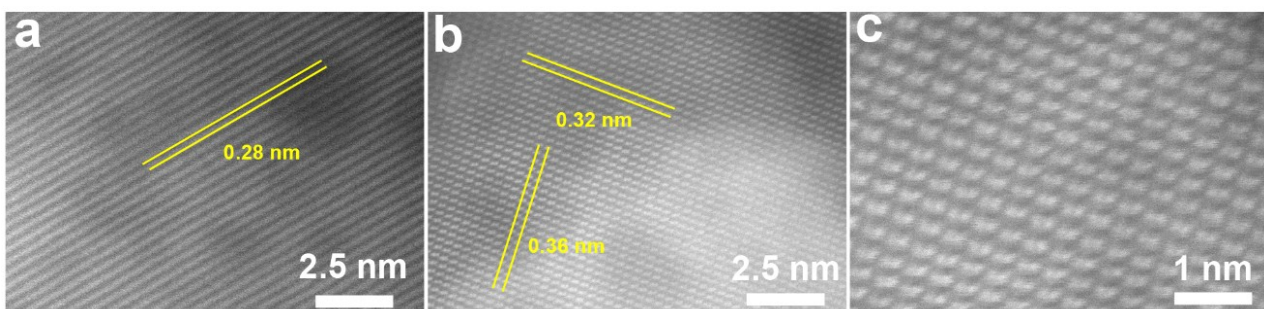


**Figure S6.** The STEM images of  $\text{ZrO}_2$  after annealing at 700 °C for different positions. The lattice fringes of 0.28, 0.32 and 0.36 nm are assigned to the (111),  $(\bar{1}\bar{1}1)$  and (110) planes of monoclinic  $\text{ZrO}_2$  (JCPDS card no. 37-1484), respectively.

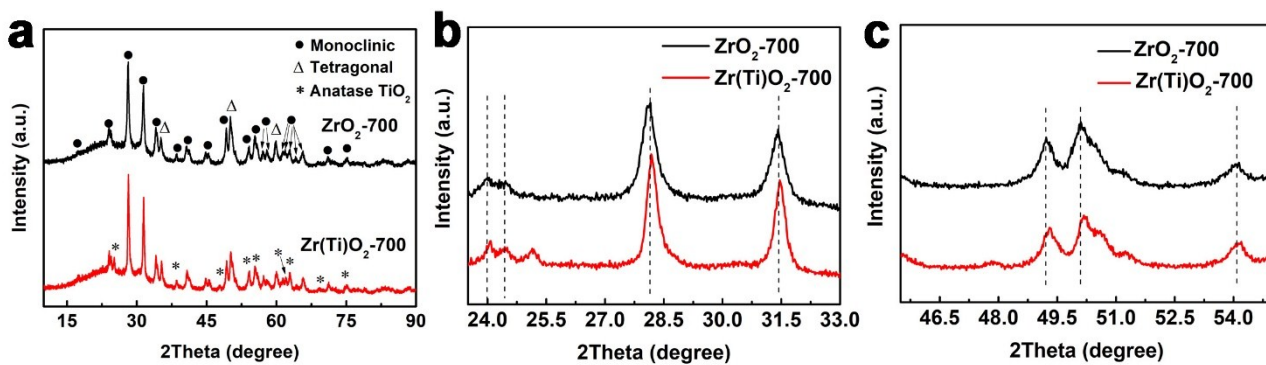


**Figure S7.** XRD patterns of ZrO<sub>2</sub> and Zr(Ti)O<sub>2</sub> after annealing at 700 °C (a). Local regions for  $2\theta$  values of 23.0–33.0° (b) and 45.0–55.0° (c), in which the peak shift is clearly visible.

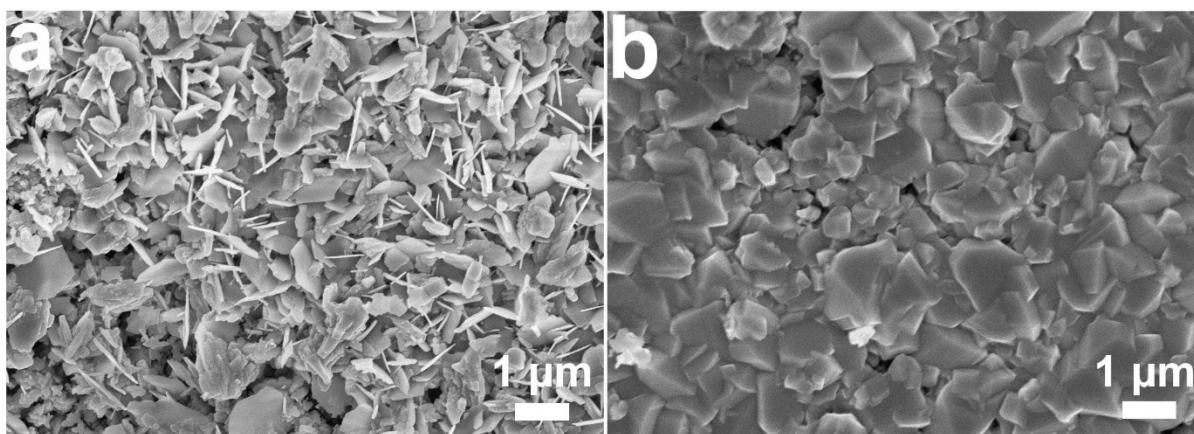


**Figure S8.** The surface (a) and bottom (b) FESEM images of Zr(Ti)O<sub>2</sub> membrane after annealing at 700 °C.

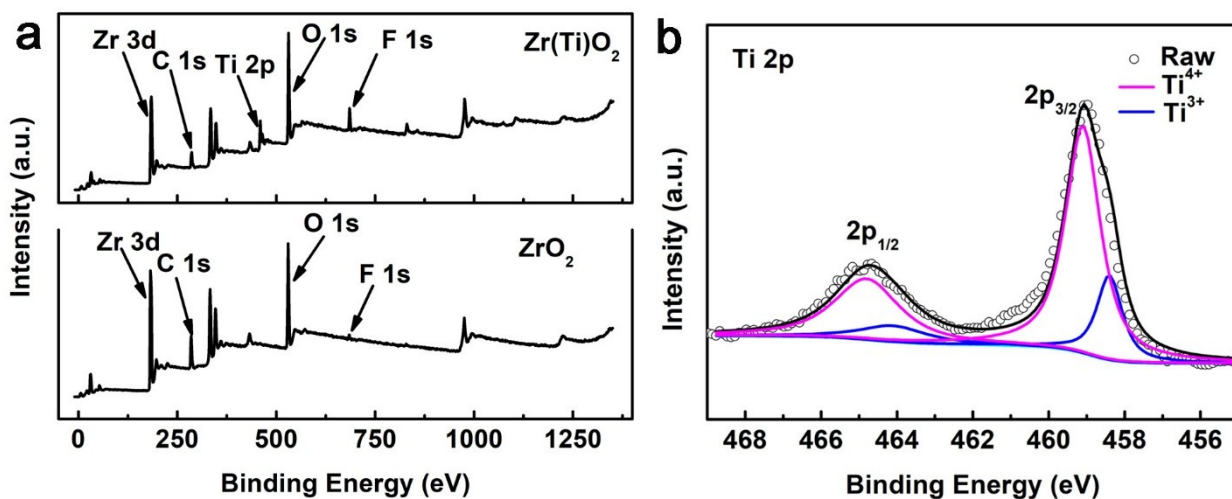


**Figure S9.** The XPS spectra of  $\text{ZrO}_2$  and  $\text{Zr(Ti)O}_2$ : Survey scan (a), and Ti 2p core levels (b).

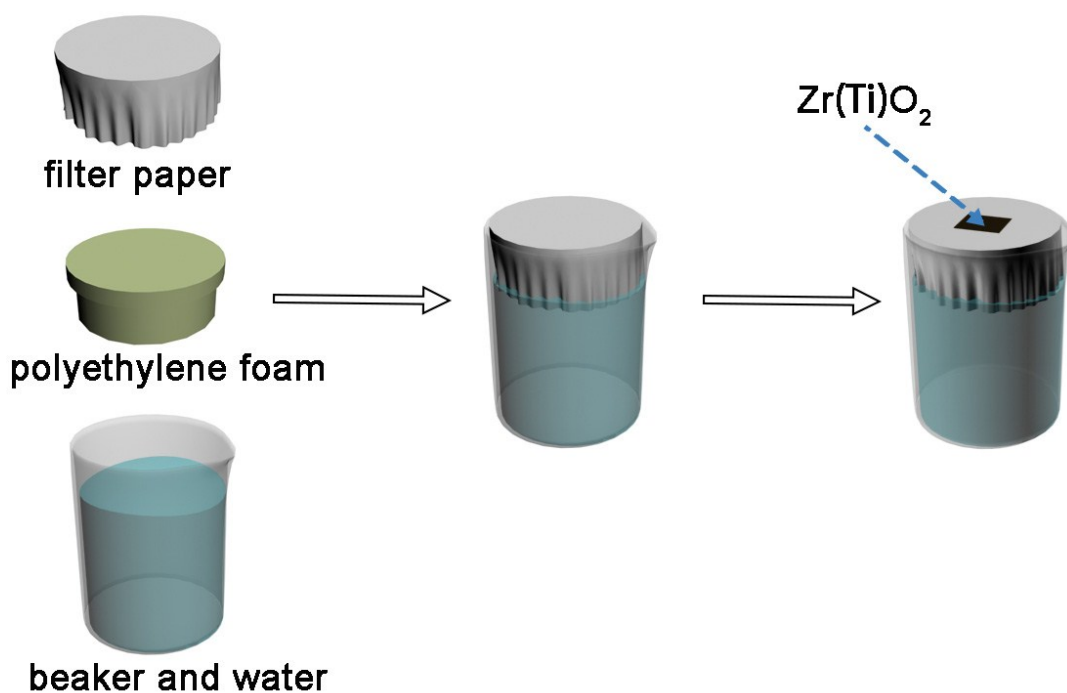


**Figure S10.** The schematic of the solar water evaporation device used in this study.

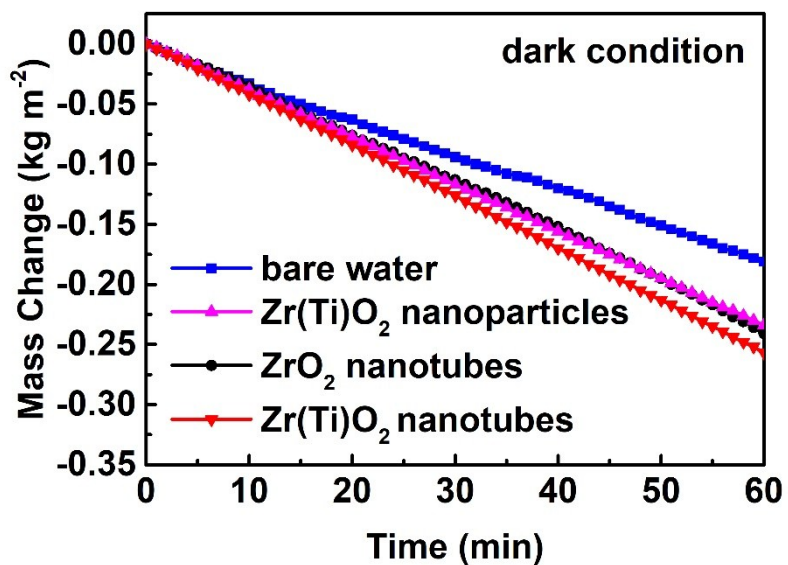


**Figure S11.** The mass change of different materials under dark condition at 20.5 °C and 40% relative humidity.

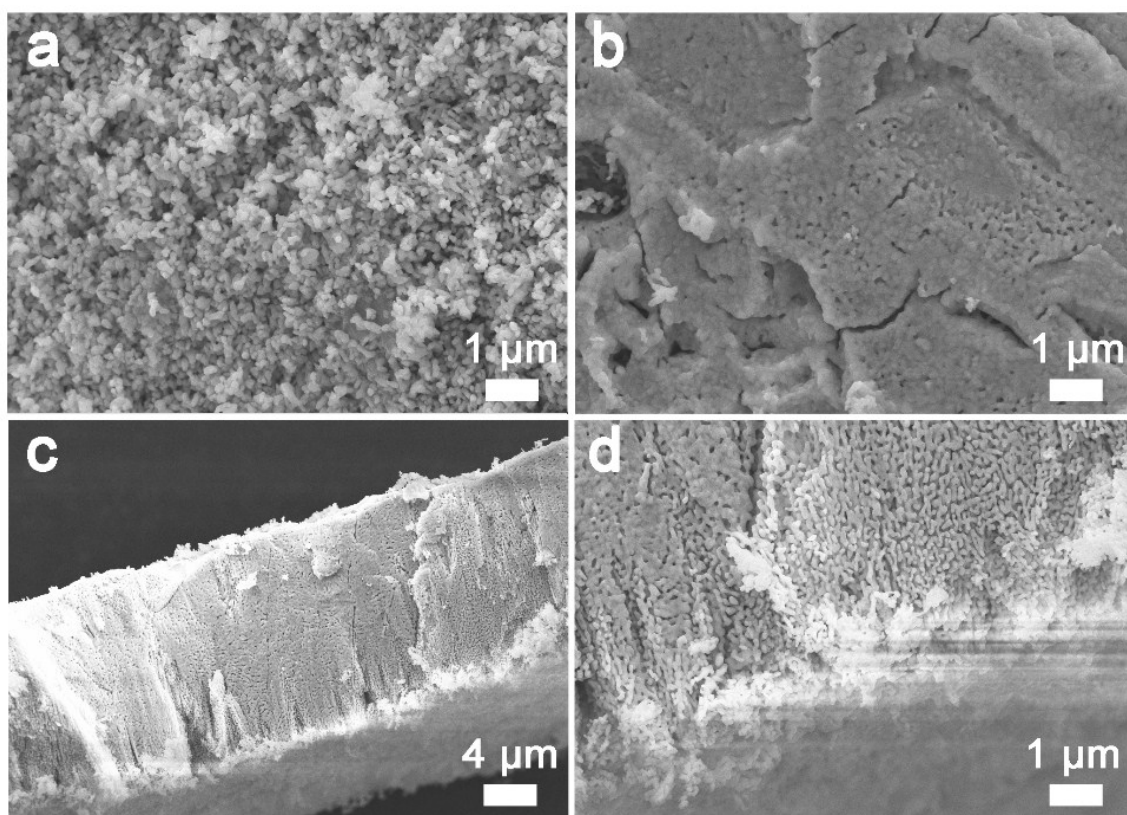


**Figure S12.** Surface (a), bottom (b), and cross-sectional (c, d) FESEM images of Zr(Ti)O<sub>2</sub> nanoparticles membranes; (d) is a local magnification in (c).

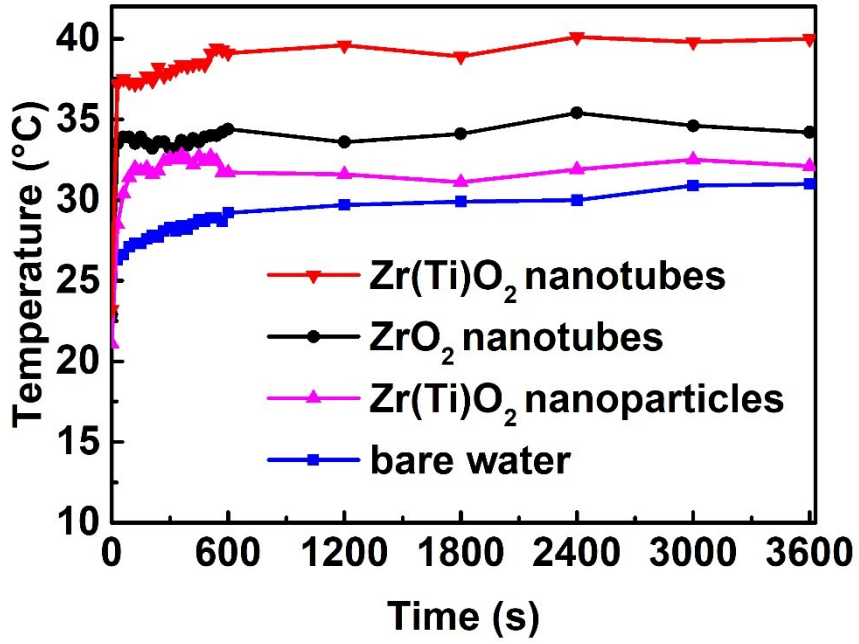


**Figure S13.** Surface temperature as a function of time for Zr(Ti)O<sub>2</sub> nanotubes, ZrO<sub>2</sub> nanotubes, Zr(Ti)O<sub>2</sub> nanoparticles, and bare water under AM 1.5g solar irradiation at 1 kW m<sup>-2</sup>.

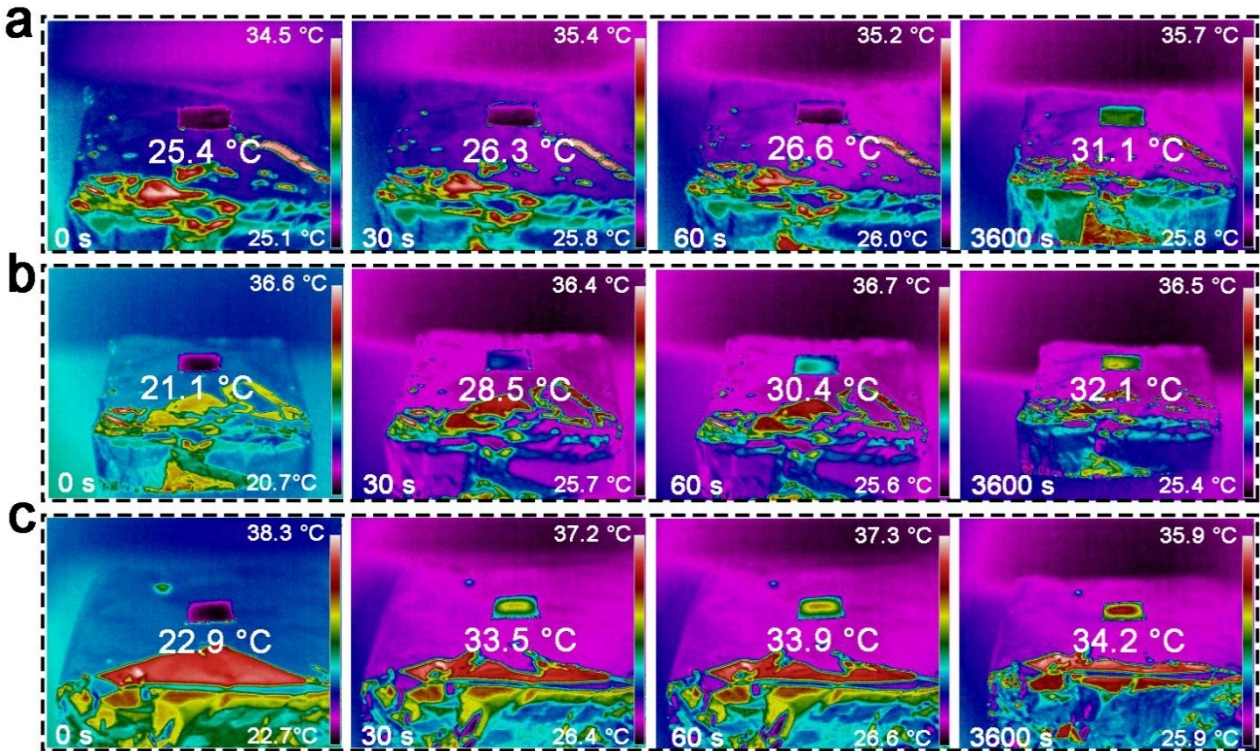


**Figure S14.** Infrared thermal images of bare water (a), Zr(Ti)O<sub>2</sub> nanoparticle (b) and ZrO<sub>2</sub> nanotube (c) devices under AM1.5g solar irradiation for different durations.



Figure S15. Evaluation of water purity using a multimeter with a constant distance between electrodes.

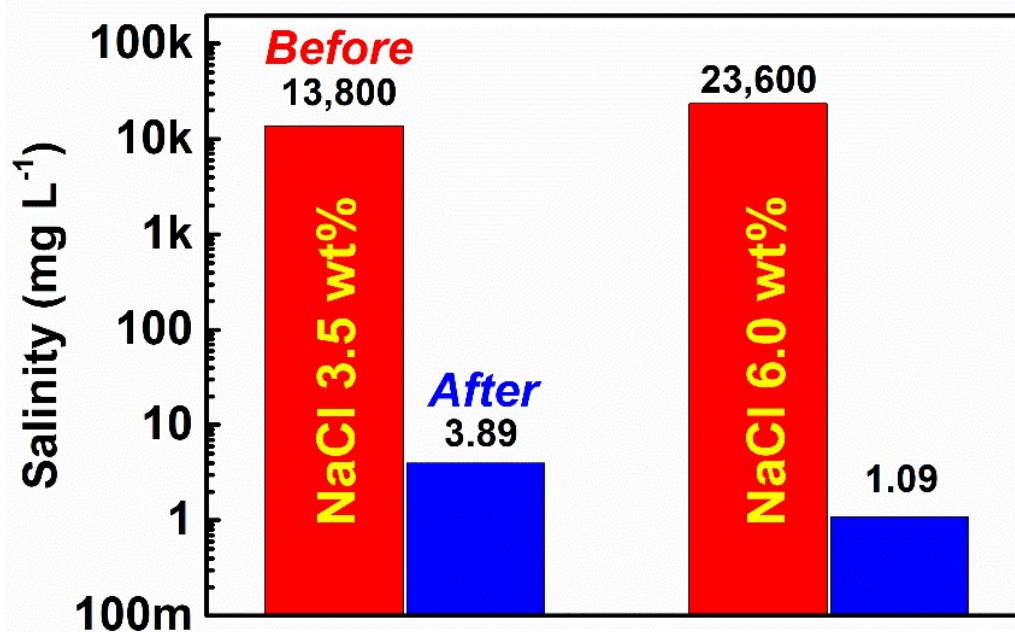
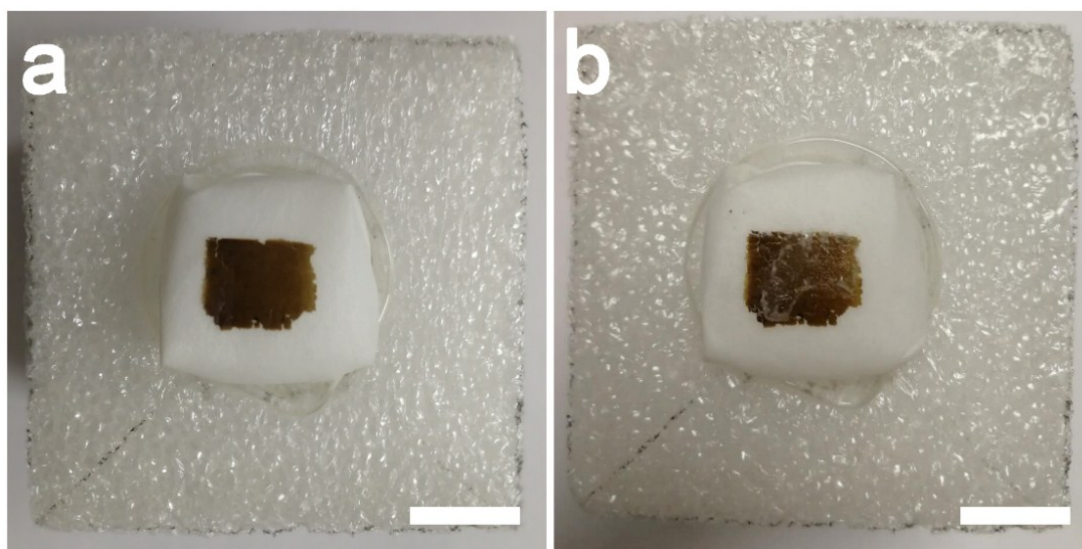
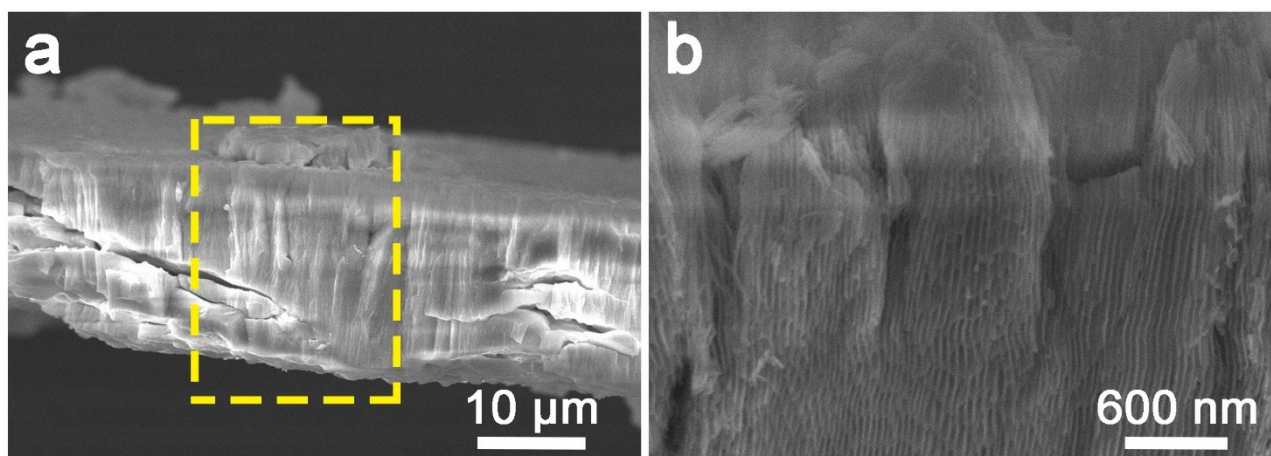


Figure S16. Salinities of different NaCl solutions and the corresponding purified water.



**Figure S17.** Optical photographs of the  $\text{Zr(Ti)O}_2$  evaporator before (a) and after (b) solar irradiation for 5 h. Scale bar is 1 cm. A few salt crystals can be observed at the membrane surface after irradiation.



**Figure S18.** Cross-sectional SEM images of  $\text{Zr(Ti)O}_2$  membranes after desalination of 6.00 wt% NaCl solution (a), where (b) is a local magnification in (a). The rectangular region was used for EDX examination and the relevant results are shown in **Table S3**.

**Table S3.** The EDX results of Zr(Ti)O<sub>2</sub> membranes after desalination of 6.00 wt% NaCl solution.

Elements	O-K	C-K	Zr-L	Ti-K	Na-K	Cl-K
C atom. (at%)	37.64	48.48	6.57	2.79	2.89	1.63
C norm. (wt%)	29.50	28.52	29.35	6.55	3.26	2.83

**Table S4.** The state-of-the-art reports of solar water evaporation.

Evaporation rate (kg m <sup>-2</sup> h <sup>-1</sup> )	Evaporation temperature (°C)	References	Materials
0.950	36.2	16	carbon
1.010	43.0	17	carbon
1.050	43.0	18	carbon
1.140	39.5	19	carbon
1.210	38.8	20	carbon
1.277	38.0	21	carbon
1.286	80.0	22	carbon
1.310	70.0	23	carbon
1.320	85.0	24	carbon
1.340	40.0	25	carbon
1.380	39.7	26	carbon
1.400	70.0	27	carbon
2.500	32.0	5	carbon
1.120	42.8	28	metal compound
1.130	42.0	29	metal compound
1.140	50.0	30	metal compound
1.220	32.5	31	metal compound
1.240	42.1	32	metal compound
1.300	47.9	33	metal compound
1.320	52.0	34	metal compound
1.320	32.0	35	metal compound
1.390	44.0	36	metal compound
1.400	42.8	37	metal compound
1.430	41.3	10	metal compound
1.550	51.0	38	metal compound
0.920	39.0	39	polymer
1.150	50.0	40	polymer
1.460	43.0	41	polymer
3.200	41.3	6	polymer
<b>1.640</b>	<b>40.0</b>	<b>This work</b>	<b>metal compound</b>

## Supplementary References

- 1 J. B. Priebe, J. Radnik, A. J. J. Lennox, M.-M. Pohl, M. Karnahl, D. Hollmann, K. Grabow, U. Bentrup, H. Junge, M. Beller and A. Brückner, *ACS Catal.*, 2015, **5**, 2137-2148.
- 2 J. VandeVondele, M. Krack, F. Mohamed, M. Parrinello, T. Chassaing and J. Hutter, *Comput. Phys. Commun.*, 2005, **167**, 103-128.
- 3 S. T. Goedecker, M.; Hutter, J., *Phys. Rev. B*, 1996, **54**, 1703-1710.
- 4 J. VandeVondele and J. Hutter, *J. Chem. Phys.*, 2007, **127**, 114105.
- 5 X. Zhou, F. Zhao, Y. Guo, Y. Zhang and G. Yu, *Energy & Environmental Science*, 2018, DOI: 10.1039/c8ee00567b.
- 6 F. Zhao, X. Zhou, Y. Shi, X. Qian, M. Alexander, X. Zhao, S. Mendez, R. Yang, L. Qu and G. Yu, *Nat. Nanotechnol.*, 2018, **13**, 489-495.
- 7 F. Gong, H. Li, W. Wang, J. Huang, D. Xia, J. Liao, M. Wu and D. V. Papavassiliou, *Nano Energy*, 2019, **58**, 322-330.
- 8 L. Sun, J. Liu, Y. Zhao, J. Xu and Y. Li, *Carbon*, 2019, **145**, 352-358.
- 9 X. Wang, Q. Liu, S. Wu, B. Xu and H. Xu, *Adv. Mater.*, 2019, DOI: 10.1002/adma.201807716, e1807716.
- 10 K. Yin, S. Yang, J. Wu, Y. Li, D. Chu, J. He and J.-A. Duan, *J. Mater. Chem. A*, 2019, DOI: 10.1039/c9ta00291j.
- 11 F. P. Incropera, A. S. Lavine, T. L. Bergman and D. P. DeWitt, *Fundamentals of heat and mass transfer*, Wiley, 2007.
- 12 H. Yan and H. Guo, *Phys. Rev. E Stat. Nonlin. Soft Matter Phys.*, 2012, **85**, 011146.
- 13 R. Ranjbarzadeh, A. H. Meghdadi Isfahani, M. Afrand, A. Karimipour and M. Hojaji, *Appl. Therm. Eng.*, 2017, **125**, 69-79.
- 14 K. S. Hwang, S. P. Jang and S. U. S. Choi, *Int. J. Heat Mass Tran.*, 2009, **52**, 193-199.
- 15 M. R. Esfahani, E. M. Languri and M. R. Nunna, *Int. Commun. Heat Mass*, 2016, **76**, 308-315.
- 16 C. Chen, Y. Li, J. Song, Z. Yang, Y. Kuang, E. Hitz, C. Jia, A. Gong, F. Jiang, J. Y. Zhu, B.

- Yang, J. Xie and L. Hu, *Adv. Mater.*, 2017, **29**, 1701756.
- 17 V. Kashyap, A. Al-Bayati, S. M. Sajadi, P. Irajizad, S. H. Wang and H. Ghasemi, *J. Mater. Chem. A*, 2017, **5**, 15227-15234.
- 18 G. Xue, K. Liu, Q. Chen, P. Yang, J. Li, T. Ding, J. Duan, B. Qi and J. Zhou, *ACS Appl. Mater. Interfaces*, 2017, **9**, 15052-15057.
- 19 A. Guo, X. Ming, Y. Fu, G. Wang and X. Wang, *ACS Appl. Mater. Interfaces*, 2017, **9**, 29958-29964.
- 20 X. Li, W. Xu, M. Tang, L. Zhou, B. Zhu, S. Zhu and J. Zhu, *Proc. Natl. Acad. Sci. USA.*, 2016, **113**, 13953-13958.
- 21 N. Xu, X. Hu, W. Xu, X. Li, L. Zhou, S. Zhu and J. Zhu, *Adv. Mater.*, 2017, **29**.
- 22 Z. Wang, Q. Ye, X. Liang, J. Xu, C. Chang, C. Song, W. Shang, J. Wu, P. Tao and T. Deng, *J. Mater. Chem. A*, 2017, **5**, 16359-16368.
- 23 Y. Wang, L. Zhang and P. Wang, *ACS Sustain. Chem. Eng.*, 2016, **4**, 1223-1230.
- 24 L. Shi, Y. Wang, L. Zhang and P. Wang, *J. Mater. Chem. A*, 2017, **5**, 16212-16219.
- 25 X. Hu, W. Xu, L. Zhou, Y. Tan, Y. Wang, S. Zhu and J. Zhu, *Adv. Mater.*, 2017, **29**.
- 26 P. Zhang, J. Li, L. Lv, Y. Zhao and L. Qu, *ACS Nano*, 2017, **11**, 5087-5093.
- 27 H. Ren, M. Tang, B. Guan, K. Wang, J. Yang, F. Wang, M. Wang, J. Shan, Z. Chen, D. Wei, H. Peng and Z. Liu, *Adv. Mater.*, 2017, **29**.
- 28 Z. Guo, X. Ming, G. Wang, B. Hou, X. Liu, T. Mei, J. Li, J. Wang and X. Wang, *Semicond. Sci. Technol.*, 2018, **33**, 025008.
- 29 H. Liu, X. Zhang, Z. Hong, Z. Pu, Q. Yao, J. Shi, G. Yang, B. Mi, B. Yang, X. Liu, H. Jiang and X. Hu, *Nano Energy*, 2017, **42**, 115-121.
- 30 L. Zhang, J. Xing, X. Wen, J. Chai, S. Wang and Q. Xiong, *Nanoscale*, 2017, **9**, 12843-12849.
- 31 Y. Xu, J. Ma, Y. Han, J. Zhang, F. Cui, Y. Zhao, X. Li and W. Wang, *ACS Sustain. Chem. Eng.*, 2019, **7**, 5476-5485.
- 32 G. Song, Y. Yuan, J. Liu, Q. Liu, W. Zhang, J. Fang, J. Gu, D. Ma and D. Zhang, *Advanced*

- Sustainable Systems*, 2019, DOI: 10.1002/adsu.201900003, 1900003.
- 33 D. Wu, D. Qu, W. Jiang, G. Chen, L. An, C. Zhuang and Z. Sun, *J. Mater. Chem. A*, 2019, DOI: 10.1039/c9ta00529c.
- 34 J. Wang, Y. Li, L. Deng, N. Wei, Y. Weng, S. Dong, D. Qi, J. Qiu, X. Chen and T. Wu, *Adv. Mater.*, 2017, **29**.
- 35 M. Chen, Y. Wu, W. Song, Y. Mo, X. Lin, Q. He and B. Guo, *Nanoscale*, 2018, **10**.
- 36 J. Fang, Q. L. Liu, W. Zhang, J. J. Gu, Y. S. Su, H. L. Su, C. P. Guo and D. Zhang, *J. Mater. Chem. A*, 2017, **5**, 17817-17821.
- 37 L. Shi, Y. Shi, S. Zhuo, C. Zhang, Y. Aldrees, S. Aleid and P. Wang, *Nano Energy*, 2019, **60**, 222-230.
- 38 L. Zhu, L. Sun, H. Zhang, D. Yu, H. Aslan, J. Zhao, Z. Li, M. Yu, F. Besenbacher and Y. Sun, *Nano Energy*, 2019, **57**, 842-850.
- 39 L. Zhang, B. Tang, J. Wu, R. Li and P. Wang, *Adv. Mater.*, 2015, **27**, 4889-4894.
- 40 X. Huang, Y.-H. Yu, Oscar L. de Llergo, S. M. Marquez and Z. Cheng, *RSC Adv.*, 2017, **7**, 9495-9499.
- 41 C. Li, D. Jiang, B. Huo, M. Ding, C. Huang, D. Jia, H. Li, C. Liu and J. Liu, *Nano Energy*, 2019, DOI: 10.1016/j.nanoen.2019.03.087.